ZAMM · Z. Angew. Math. Mech. **89**, No. 7, 552 – 569 (2009) / **DOI** 10.1002/zamm.200800218

A numerical study for linear isotropic Cosserat elasticity with conformally invariant curvature

Jena Jeong[1,*], **Hamidréza Ramézani**[2,**], **Ingo Münch**[3,***], **and Patrizio Neff** [4,****]

[1] École Spéciale des Travaux Publics, du Bâtiment et de l'industrie (ESTP), 28 avenue du Président Wilson, 94234 Cachan Cedex, France
[2] École Polytechnique de l'Université d'Orléans, CNRS-CRMD, 8 rue Léonrad de Vinci, 45072 Orléans, France
[3] Institut für Baustatik, Universität Karlsruhe (TH), Kaiserstr. 12, 76131 Karlsruhe, Germany
[4] Lehrstuhl für Nichtlineare Analysis und Modellierung, Fachbereich Mathematik, Universität Duisburg-Essen, Universitätsstraße 2, 45141 Essen, Germany

Received 18 December 2008, revised 26 April 2009, accepted 14 May 2009
Published online 7 July 2009

Key words Polar-materials, microstructure, conformal transformations, structured continua, solid mechanics, FEM.
MSC (2000) 74A35, 74A30, 74C05, 74C10, 74C20, 74D10, 74E05, 74E10, 74E15, 74E20, 74G30, 74G65, 74N15

We investigate the numerical response of the linear Cosserat model with conformal curvature. In our simulations we compare the standard Cosserat model with a novel conformal Cosserat model in torsion and highlight its intriguing features. In all cases, free boundary conditions for the microrotations $\overline{A}$ are applied. The size-effect response is markedly changed for the novel curvature expression. Our results suggest that the Cosserat couple modulus $\mu_c > 0$ remains a true material parameter independent of the sample size which is impossible for stronger, pointwise positive curvature expressions.

1 Introduction

The Cosserat continuum falls into the group of generalized continua which have the capacity to take into account size-effects in a natural manner. The Cosserat model is one of the most prominent extended continuum models. It has emerged from the work of the brothers François and Eugène Cosserat [1, 2] at the turn of the last century. Their originally nonlinear, geometrically exact development has been largely forgotten for decades only to be rediscovered in a restricted linearized setting in the early sixties by Günther [3], Mindlin [4–9], and Eringen [10–13]. Since then, the original Cosserat concept has been generalized in various directions, notably by Eringen and his coworkers who extended the Cosserat concept to include also microinertia effects and to rename it subsequently into micropolar theory [14–16][1].

The Cosserat theory has been also applied to the human bone [19,20] in the biomechanics branch, foams [21–25] (Lakes' benchmark papers) for the man-made materials or so-called synthetic materials, cellular solids [26], and composites [27] . Some particular applications can be addressed to the metallic foams for energy saving purposes and Voronoi cells [28–30]. Forest et al. made benchmark contributions in the incremental analysis, finite deformation, strain gradient theory, and homogenization aspects for the polycrystalline materials [31–39]. There are also some studies pertaining to the elasto-plasticity of the Cosserat-based media, e.g. Ristinmaa et al. for the couple stress plasticity [40] and Neff based on an original Cosserat concept (geometrically exact Cosserat non linear). The infinitesimal and finite elastic-plastic Cosserat theory have been fully investigated [41, 42]. It is helpful to mention that the most generalized case, i.e., micromorphic case is also treated and some analytical and 2D numerical analyses are available in the open literature [43–45]. The Cosserat model includes in a natural way size effects, i.e., small samples behave comparatively stiffer than large samples. In classical, size-independent models this would lead to an apparent increase of elastic moduli for smaller samples of the same material. Compared to classical linear elasticity the model features three additional, independent degrees of freedom, related to the independent rotation of each particle. In the simplest linear isotropic case, one coupling constant, here called Cosserat

* Corresponding author E-mail: jeong@profs.estp.fr
** E-mail: hamidreza.ramezani@univ-orleans.fr
*** E-mail: im@bs.uka.de
**** E-mail: patrizio.neff@uni-due.de

[1] Some of Eringen's notations have been revised and corrected later on by Cowin [17] and by Eringen himself [14–16]. The original notations make some flaws and it should be carefully taken into account by the relevant Cosserat moduli or Cosserat material constants [18].

couple modulus $\mu_c \geq 0$ and three internal length scale parameters α, β, γ need to be determined in addition to the two classical Lamé-constants μ, λ [2] . See [43, 46–48] for an in-depth discussion of mathematical and modelling aspects of the Cosserat model.[3]

In this work we will discuss the finite-element simulation of the linear Cosserat model with a hitherto not considered set of parameter values, called the conformal Cosserat case. The finite element analysis of Cosserat materials has already been studied in the literature. Early works on the finite element analysis based on the Cosserat theory are those done by Baluch [49] and Nakamura [50] in which a simple three-node triangle element with three degrees of freedom at each node is used for a two-dimensional problem. A higher-order triangle element again for a two-dimensional analysis based on Cosserat elasticity has been recently proposed by Providas [51], and Trovalusci et al. [52] treats the 2D-nonlinear case. The Cosserat theory has also been employed by Nadler and Rubin to formulate a three-dimensional finite element for dynamic analysis in nonlinear elasticity [53]. In addition, higher-order elements for elastic analysis of shells have been proposed by Jog [54]. Though several numerical studies have been conducted for Cosserat materials only few of them treat the full three-dimensional case. The two-dimensional Cosserat setting automatically removes two material parameters and the altogether required Cosserat material moduli reduce to only four (the two-dimensional problem is much simpler because of a fixed axis of rotations). An example calculation of the linear isotropic Cosserat model for two-dimensional finite elements has been performed by Li et al. [55]. There are also some studies in the literature for foams [40, 56–61]. Huang et al. [62], Zastrau et al. [63, 64] have done very early attempts based on the Cosserat curvature parameter choice $\alpha = \beta = 0$, $\gamma > 0$ and $\beta = \gamma > 0$, $\alpha \geq 0$, respectively (see Eq. (1.3) for its meaning). Zastrau thus arrives at the symmetry of the couple stress tensor m, a choice which has also been advocated as early as [65, 66]. Recently, the symmetry of the couple stress tensor has been motivated in [67] for the constraint couple stress model (the indeterminate couple stress model). In some cases, the algorithms are already extended to micropolar elasto-plastic problems, see, e.g. [42, 68–70]. First steps in the much more involved geometrically exact direction are taken in [71, 72].

While we have a geometrically exact 3D-code successfully running [71] we present here only the "linear" version for mainly two reasons: first, other groups do not necessarily have access to a 3D-geometrically exact code, making comparison impossible, and second, we investigate a novel situation, called the *conformal curvature case*, where already the linear response shows interesting features. Moreover, we solely concentrate on fully three-dimensional finite element models. Particularly, we focus on the torsion test with a cylindrical bar whose implementation helps us to take into account more pronounced size effects comparing to the simple tension, compression or three points bending test. Based on the companion paper [73] on the underlying theory of the conformal Cosserat model, we infer that the weakest mathematically possible curvature energy assumption, still leading to a well-posed model, is a good choice. This is the conformal curvature case. This not only reduces the needed Cosserat material moduli but also removes material moduli dependency problems which usually takes place for the stronger curvature energy assumption (pointwise positive "classical" case). By taking advantage of these theoretical findings we are motivated to put them into practice via our numerical experiments. As will be presented in the next sections, these experiments confirm the analytical aspects [73] and provide a deep landscape on the Cosserat modeling and simulation issues.

Our paper is now organized as follows. First, we recall the variational setting of the Cosserat model, we present the weak form of the equations and give a classification for the Cosserat model introducing our novel conformal case. Then we establish universal analytical solutions for linear elasticity and conformal Cosserat elasticity which are further on used for the validation of our implementation. We present some details of our implementation and further validate it against the classical analytical torsion solution and other limit cases: linear elasticity and constant infinitesimal mean rotation. Having thus demonstrated the suitability of our method we turn to the detailed investigation of size-effects in torsion for the different Cosserat curvature settings. The notation is the same as in the companion paper [73].

Let us begin by establishing the linear Cosserat model along with some of our notation. This section does not contain new results.

---

[2] To avoid any conflict among the available Cosserat moduli, we use the Neff's formulations [46] which contain some corrections provided by Cowin [17] and by Eringen himself [14–16]. Then, we can write the following relations:

$$\ell_b{}^2 := \frac{\gamma}{2(2\mu^* + \kappa)} \quad \text{and} \quad \ell_t{}^2 := \frac{\beta + \gamma}{2\mu^* + \kappa} \,, \tag{1.1a}$$

$$N^2 := \frac{\mu_c}{\mu + \mu_c} = \frac{\kappa}{2(\mu^* + \kappa)} \,, \quad \text{where} \quad 0 \leq N^2 \leq 1 \,, \tag{1.1b}$$

$$\Psi := \frac{\beta + \gamma}{\alpha + \beta + \gamma} \,, \quad \text{where} \quad 0 \leq \Psi \leq \frac{3}{2} \,, \tag{1.1c}$$

where, κ and μ^* are the Cosserat couple modulus and Pseudo-Lamé's constant in accordance with the Eringen's notation.

[3] See also http://www.mathematik.tu-darmstadt.de/fbereiche/analysis/pde/staff/neff/patrizio/Cosserat.html

1.1 The linear elastic Cosserat model in variational form

For the **displacement** $u : \Omega \subset \mathbb{R}^3 \mapsto \mathbb{R}^3$ and the **skew-symmetric infinitesimal microrotation** $\overline{A} : \Omega \subset \mathbb{R}^3 \mapsto \mathfrak{so}(3)$ we consider the **two-field** minimization problem

$$I(u, \overline{A}) = \int_\Omega W_{\rm mp}(\overline{\varepsilon}) + W_{\rm curv}(\nabla \operatorname{axl} \overline{A}) - \langle f, u\rangle - \langle M, \phi\rangle \, {\rm dV}$$
$$- \int_{\partial\Omega} \langle f_s, u\rangle + \langle M_s, u\rangle \, {\rm dS} \mapsto \quad \min . \text{ w.r.t. } (u, \overline{A}) \,, \tag{1.2}$$

under the following constitutive requirements and boundary conditions

$$\overline{\varepsilon} = \nabla u - \overline{A}, \quad \textbf{first Cosserat stretch tensor}$$
$$u_{|\Gamma} = u_{\rm d} \,, \quad \textbf{essential displacement boundary conditions}$$
$$W_{\rm mp}(\overline{\varepsilon}) = \mu \, \| \operatorname{sym} \overline{\varepsilon} \|^2 + \mu_c \, \| \operatorname{skew} \overline{\varepsilon} \|^2 + \frac{\lambda}{2} \operatorname{tr} [\operatorname{sym} \overline{\varepsilon}]^2 \,, \qquad \textbf{strain energy} \tag{1.3}$$
$$\phi := \operatorname{axl} \overline{A} \in \mathbb{R}^3, \quad \overline{\mathfrak{k}} = \nabla \phi \,, \quad \| \operatorname{curl} \phi \|^2_{\mathbb{R}^3} = 4 \| \operatorname{axl} \operatorname{skew} \nabla \phi \|^2_{\mathbb{R}^3} = 2 \| \operatorname{skew} \nabla \phi \|^2_{\mathbb{M}^{3\times 3}} \,,$$
$$W_{\rm curv}(\nabla \phi) = \frac{\gamma + \beta}{2} \| \operatorname{dev} \operatorname{sym} \nabla \phi \|^2 + \frac{\gamma - \beta}{2} \| \operatorname{skew} \nabla \phi \|^2 + \frac{3\alpha + (\beta + \gamma)}{6} \operatorname{tr} [\nabla \phi]^2 \,.$$

Here, f are given volume forces while $u_{\rm d}$ are Dirichlet boundary conditions[4] for the displacement at $\Gamma \subset \partial\Omega$ where $\Omega \subset \mathbb{R}^3$ denotes a bounded Lipschitz domain. Surface tractions, volume couples, and surface couples can be included in the standard way. The strain energy $W_{\rm mp}$ and the curvature energy $W_{\rm curv}$ are the most general isotropic quadratic forms in the **infinitesimal non-symmetric first Cosserat strain tensor** $\overline{\varepsilon} = \nabla u - \overline{A}$ and the **micropolar curvature tensor** $\overline{\mathfrak{k}} = \nabla \operatorname{axl} \overline{A} = \nabla \phi$ (curvature-twist tensor). The parameters μ, λ[MPa] are the classical Lamé moduli and α, β, γ are further micropolar moduli with dimension $[\text{Pa} \cdot \text{m}^2] = [\text{N}]$ of a force. The additional parameter $\mu_c \geq 0$[MPa] in the strain energy is the **Cosserat couple modulus**. For $\mu_c = 0$ the two fields of displacement u and microrotations $\overline{A} \in \mathfrak{so}(3)$ decouple and one is left formally with classical linear elasticity for the displacement u. Lakes has treated a related degenerate limit case in [74].

1.2 The weak form of the equilibrium balance equations

Let us recall the kinematic relation

$$\overline{\varepsilon} = \nabla u - \overline{A} \quad \text{with} \quad \overline{A}_{ij} = -\varepsilon_{ijk} \phi_k, \tag{1.4}$$

along with the definition of the stress tensor σ and the couple stress tensor (moment stress tensor) m

$$\sigma = \frac{\partial W_{\rm mp}(\overline{\varepsilon})}{\partial \overline{\varepsilon}} \,, \qquad m = \frac{\partial W_{\rm curv}(\nabla \phi)}{\partial \nabla \phi} \,. \tag{1.5}$$

The internal potential, Ψ_{int}, which is a functional of the non-symmetric infinitesimal Cosserat strain and curvature strain can be written as:

$$\Psi_{\rm int}(u, \overline{A}) = \int_\Omega W_{\rm mp}(\overline{\varepsilon}) + W_{\rm curv}(\nabla \phi) \, {\rm dV}. \tag{1.6}$$

Let $\Psi_{\rm ext}$ define the external virtual work as below:

$$\Psi_{\rm ext}(u, \overline{A}) = \int_\Omega \langle f, u\rangle + \langle M, \phi\rangle \, {\rm dV} + \int_{\partial\Omega} \langle f_s, u\rangle + \langle M_s, \phi\rangle \, {\rm dS} \,, \tag{1.7}$$

where f and M are the external body force and body moment. Moreover, f_s and M_s are the stress vector and couple stress vector, respectively. Taking variations of the energy in (1.6) w.r.t. both displacement $u \in \mathbb{R}^3$ and infinitesimal microrotation $\overline{A} \in \mathfrak{so}(3)$ we arrive at the weak form of equilibrium system (the Euler-Lagrange equations of (1.2))

$$\delta \Psi_{\rm int} - \delta \Psi_{\rm ext} = 0 \tag{1.8}$$

[4] Note that it is always possible to prescribe essential boundary values for the microrotations $\overline{A}$ but we use Neumann conditions for microrotations everywhere to the effect that $m.\vec{n} = 0$ on $\partial\Omega$.

with

$$\delta\Psi_{\rm int} = \int_\Omega \langle D_{\overline{\varepsilon}} W_{\rm mp}(\overline{\varepsilon}), \delta\overline{\varepsilon}\rangle + \langle D_{\nabla\phi} W_{\rm curv}(\nabla\phi), \nabla\delta\phi\rangle \, {\rm dV}\,, \tag{1.9}$$

where $\delta\overline{\varepsilon} = \delta u - \delta\overline{A}$ is understood. With substitution of (1.9) and (1.7) into (1.8), the following equation is easily derived:

$$\int_\Omega \langle \sigma, \delta\overline{\varepsilon}\rangle + \langle m, \nabla\delta\phi\rangle \, {\rm dV} - \int_\Omega \langle f, \delta u\rangle + \langle M, \delta\phi\rangle \, {\rm dV} - \int_{\partial\Omega} \langle f_s, \delta u\rangle + \langle M_s, \delta\phi\rangle \, {\rm dS} = 0\,. \tag{1.10}$$

The virtual displacement δu is conjugate to the external force and the virtual rotation vector $\delta\phi$ to the external moment. This weak form is the basis for our numerical simulations.

1.3 The strong form of the linear elastic Cosserat balance equations

Going one step further, we collect also the balance equations in strong form for our subsequent classification of the Cosserat model. Sorting (1.10) w.r.t. δu and $\delta\phi$ and using integration by parts we obtain

$$\begin{aligned}
{\rm Div}\,\sigma &= f\,, \qquad \textbf{balance of linear momentum}\\
-{\rm Div}\, m &= 4\,\mu_c \cdot {\rm axl}\,{\rm skew}\,\overline{\varepsilon}\,, \quad \textbf{balance of angular momentum}\\
\sigma &= 2\mu \cdot {\rm sym}\,\overline{\varepsilon} + 2\mu_c \cdot {\rm skew}\,\overline{\varepsilon} + \lambda \cdot {\rm tr}\,[\overline{\varepsilon}] \cdot 1\!\!1 = (\mu+\mu_c)\cdot\overline{\varepsilon} + (\mu-\mu_c)\cdot\overline{\varepsilon}^T + \lambda\cdot{\rm tr}\,[\overline{\varepsilon}]\cdot 1\!\!1\\
&= 2\mu \cdot {\rm dev}\,{\rm sym}\,\overline{\varepsilon} + 2\mu_c \cdot {\rm skew}\,\overline{\varepsilon} + K \cdot {\rm tr}\,[\overline{\varepsilon}] \cdot 1\!\!1\,,\\
m &= (\gamma+\beta)\ {\rm dev}\,{\rm sym}\,\nabla\phi + (\gamma-\beta)\ {\rm skew}\,\nabla\phi + \frac{3\alpha+(\gamma+\beta)}{2}\,{\rm tr}\,[\nabla\phi]\,1\!\!1\,,\\
\phi &= {\rm axl}\,\overline{A}\,, \quad u_{|\rm r} = u_{\rm d}\,, \quad m.\vec{n}_{|\partial\Omega} = 0\,.
\end{aligned} \tag{1.11}$$

We run this Cosserat model with three different sets of variables for the curvature energy which in each step relaxes the curvature energy.

1: **pointwise positive case:** $(\mu L_c^2/2)\|\nabla\phi\|^2$. This corresponds to $\alpha = 0, \quad \beta = 0, \quad \gamma = \mu\, L_c^2$.
2: **symmetric case:** $(\mu L_c^2/2)\|\,{\rm sym}\,\nabla\phi\|^2$. This corresponds to $\alpha = 0,\ \beta = \gamma$, and $\gamma = (\mu\, L_c^2/2)$.
3: **conformal case:** $(\mu L_c^2/2)\|\,{\rm dev}\,{\rm sym}\,\nabla\phi\|^2 = (\mu L_c^2/2)(\|\,{\rm sym}\,\nabla\phi\|^2 - (1/3){\rm tr}\,[\nabla\phi]^2)$. This corresponds to $\beta = \gamma$ and $\gamma = (\mu\, L_c^2/2)$ and $\alpha = -(1/3)\mu\, L_c^2$.

Note that all three cases are mathematically well-posed [46, 48]. The pointwise positive case1 is usually considered. Case2 leads to a symmetric couple-stress tensor which in turn has been considered by [63, 65, 66] and case3 is the main object of our investigation. It is necessary to indicate that the Cosserat models are also motivated with a beam model [75] or so-called grid framework model [76–78].

2 Conformal transformations – universal solutions

Next we consider certain types of universal solutions, first for classical linear elasticity.

2.1 Classical Cauchy linear elasticity and conformal invariance

The stress-strain relation in isotropic linear elasticity can always be written as

$$\sigma = 2\mu \cdot {\rm dev}\,{\rm sym}\,\nabla u + K \cdot {\rm tr}\,[\nabla u] \cdot 1\!\!1\,, \tag{2.1}$$

where K is the bulk modulus. Inserting for u an **infinitesimal conformal map** $u_C : \mathbb{R}^3 \mapsto \mathbb{R}^3$ which is defined by [73]:

$$\begin{aligned}
u_C(x) &= \frac{1}{2}\left(2\langle {\rm axl}(\widehat{W}), x\rangle\, x - {\rm axl}(\widehat{W})\,\|x\|^2\right) + [\widehat{p}\,1\!\!1 + \widehat{A}].x + \widehat{b}\,,\\
\nabla u_C(x) &= {\rm anti}(\widehat{W}.x) + \langle {\rm axl}(\widehat{W}), x\rangle\, 1\!\!1 + (\widehat{p}\,1\!\!1 + \widehat{A})\,,
\end{aligned} \tag{2.2}$$

where $\widehat{W}, \widehat{A} \in \mathfrak{so}(3)$, $\widehat{b} \in \mathbb{R}^3$, and $\widehat{p} \in \mathbb{R}$ are arbitrary constants, we have for the Cauchy stress

$$\sigma(\nabla u_C) = 2\mu \cdot 0 + K \operatorname{tr}[\nabla u_C]\, 1\!\!1 = K \operatorname{tr}\left[\widehat{p} + \langle \operatorname{axl}(\widehat{W}), x\rangle\, 1\!\!1\right] 1\!\!1 = 3\,K\left(\widehat{p} + \langle \operatorname{axl}(\widehat{W}), x\rangle\right) 1\!\!1.$$

Thus $\operatorname{Div}\sigma(\nabla u_C) = 3\,K\ \operatorname{axl}(\widehat{W})$, for $\widehat{p}$ is constant and $\operatorname{Div}[\langle \widehat{k}, x\rangle 1\!\!1] = \widehat{k}$. Since the linear boundary value problem

$$\operatorname{Div}\sigma(\nabla u) = 3\,K\ \operatorname{axl}(\widehat{W})\,, \quad u_{|\Gamma}(x) = u_C(x)\,, \tag{2.3}$$

for a given constant $\widehat{W} \in \mathfrak{so}(3)$ admits a unique solution, this solution is already given by $u(x) = u_C(x)$. We have therefore obtained an inhomogeneous, three-dimensional analytical solution for the boundary value problem of linear elasticity with constant body forces $\widehat{f} = 3\,K\ \operatorname{axl}(\widehat{W})$. This solution can be profitably used to check any numerical algorithm for linear Cauchy elasticity. In our case we have considered one unit cube to check the numerical exactness obtained by us.

Remark 2.1 (Application to infinitesimal elasto-plasticity)**.** The proposed analytical solution is on the one hand quite inhomogeneous, on the other hand it holds that $\operatorname{dev}\sigma \equiv 0$. Therefore, classical numerical approaches for plasticity with von Mises flow laws should not give any plastic response since the yield stress is never reached. This can serve as a nontrivial numerical test for any algorithm for plasticity, especially, if the shear modulus $\mu(x)$ is assumed to have large spatial jumps [42, 79].

2.2 Linear Cosserat elasticity and conformal invariance

An extraordinary feature of this type of conformal solution in linear elasticity is that it is a universal solution for the Cosserat model and the indeterminate couple stress model as well, if the conformal curvature expression (case3) is used. The solution is invariant of the Cosserat coupling modulus μ_c and the internal length scale L_c.[5] To understand this claim let us consider the boundary value problem of linear Cosserat elasticity in strong form with conformal curvature (case3):

$$\operatorname{Div}\sigma(\nabla u, \overline{A}) = \widehat{f}\,, \quad -\operatorname{Div} m = 4\mu_c \cdot \operatorname{axl}(\operatorname{skew}\nabla u - \overline{A})\,, \tag{2.4}$$

$$\sigma = 2\mu \cdot \operatorname{dev}\operatorname{sym}\nabla u + 2\mu_c \cdot \operatorname{skew}(\nabla u - \overline{A}) + K \cdot \operatorname{tr}[\nabla u] \cdot 1\!\!1\,,$$

$$m = \mu\, L_c^2 \cdot \operatorname{dev}\operatorname{sym}\nabla \operatorname{axl}(\overline{A})\,, \quad u_{|\partial\Omega} = u_C\,,$$

where $\widehat{f}$ and u_C are taken from (2.1). We proceed to show that the solution of this boundary value problem is uniquely given by

$$u(x) = u_C(x)\,, \qquad \overline{A}(x) = \operatorname{anti}\left(\frac{1}{2}\operatorname{curl} u(x)\right)\,, \tag{2.5}$$

independent of $\mu(x)$, $\mu_c(x)$, and $L_c(x)$. To see this, consider

$$\operatorname{skew}(\nabla u - \overline{A}) = \operatorname{anti}(\operatorname{axl}(\operatorname{skew}\nabla u - \overline{A})) = \operatorname{anti}\left(\frac{1}{2}\operatorname{curl} u - \operatorname{axl}(\overline{A})\right)\,. \tag{2.6}$$

Choosing $\overline{A}(x) = \operatorname{anti}((1/2)\operatorname{curl} u(x))$ simplifies the equations to

$$\operatorname{Div}\sigma(\nabla u, \overline{A}) = \widehat{f}\,, \quad -\operatorname{Div} m = 0\,, \tag{2.7}$$

$$\sigma = 2\mu \cdot \operatorname{dev}\operatorname{sym}\nabla u + K \cdot \operatorname{tr}[\nabla u] \cdot 1\!\!1\,, \qquad m = \mu\, L_c^2\ \operatorname{dev}\operatorname{sym}\nabla\left(\frac{1}{2}\operatorname{curl} u(x)\right)\,.$$

Since $u = u_C$ and u_C is conformal, it follows [73] that the couple stress tensor m vanishes, thus the equation and Neumann conditions for microrotations are trivially satisfied. The remaining equation for the force stresses σ is satisfied because of (2.3). Since we have used $\overline{A}(x) = \operatorname{anti}((1/2)\operatorname{curl} u(x))$, the obtained solution is also a solution for the indeterminate couple stress problem (which corresponds formally to setting $\mu_c = \infty$).

Based on the above-mentioned constitutive equations for the stress, couple stress, and the applied conformal boundary condition on the unit cube, the numerical exactness of our algorithm for Cosserat elasticity has been also checked.

In Fig. 1, the infinitesimal conformal map u_C is taken as boundary condition and the deformed cube, computed for the conformal Cosserat model is shown, depicting the inhomogeneity of the conformal solutions. Note that it is not necessary to apply the displacement-boundary condition u_C everywhere at $\partial\Omega$ in order to obtain u_C as solution of the boundary value problem.

[5] Here, even a strong variation in shear modulus $\mu(x)$ would be allowed (as well as a strong variation in the couple modulus $\mu_c(x)$ and internal length scale $L_c(x)$. Only the bulk modulus K must be constant.

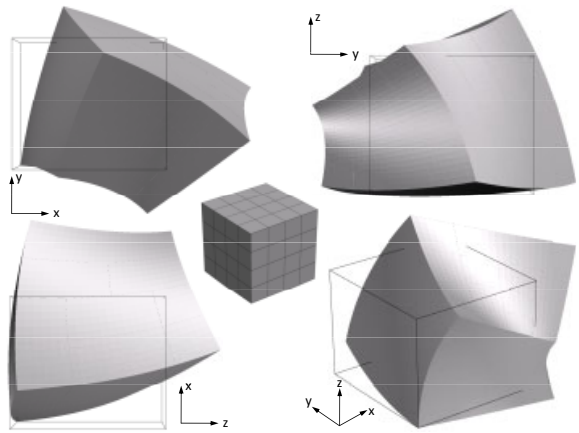

Fig. 1 Deformed and undeformed shape of the unit cube under infinitesimal conformal transformation u_C as boundary condition using the linear elastic Cosserat method and case3 assumption with $\widehat{W}_{12} = \widehat{W}_{13} = \widehat{W}_{23} = 3$, $\widehat{p} = -4$, $\widehat{A}_{12} = \widehat{A}_{13} = \widehat{A}_{23} = 4$, and $\widehat{b} = 0$, DOFs= 4300, quadratic elements.

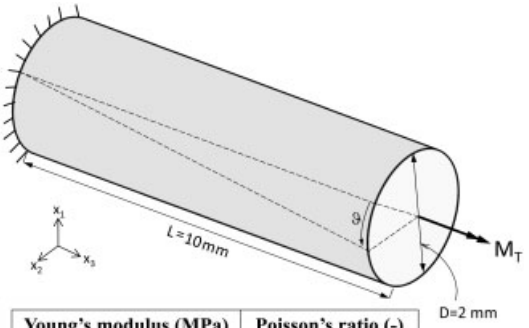

Young's modulus (MPa)	Poisson's ratio (-)
1×10^6	0.30

Fig. 2 The geometry and data of the torsion problem.

3 Configuration of a test case

3.1 Preliminaries and assumptions

The finite element method has been chosen as a relevant numerical method for the linear elastic Cosserat model. We use **isoparametric Lagrange shape functions** in our study. Moreover, we use quadratic Lagrange shape function for the displacements u and linear Lagrange shape functions for the entries of the microrotation $\overline{A} \in \mathfrak{so}(3)$. According to the discussed balance equations, there are six available state variables (three for the displacement vector u and three for the microrotation vector $\operatorname{axl}(\overline{A})$) whose computations need to be done via the coupled linear partial differential system of equations using the momentum and angular momentum balance equations based upon the weak form. We consider a cylindrical bar (diameter = 2 mm, height = 10 mm) submitted to the torsion angle ϑ at the end and choose the e_3-axis to coincide with the axis in Fig. 2, where the assumed classical, size-independent parameters E, ν can be found.

Remark 3.1 (Ansatz functions)**.** In all test cases we use quadratic ansatz functions for displacements u and linear ansatz function for microrotations $\overline{A}$. We expect a significant improvement of the accuracy of the numerical solution provided we use quadratic ansatz functions for the displacement and linear ansatz functions for the microrotations $\overline{A}$ since in the coupling term we have $\mu_c \,\|\operatorname{skew}\nabla u - \overline{A}\|^2$ whose summands thus have both the same order of approximation.

All our computations have been prepared by means of a user-written code within the general purpose FEM software COMSOL (formerly FEMLAB) [80]. We have used a parallelized direct solver making it possible to reduce the computation runtime and to enable us to utilize the full capacity of the available hardware; here an Intel-System with 32 GB memory and 8 core 3.2 GHz processor has been used. A computation with 1.029 Mi DOFs would last 25 minutes. As will be seen later, our numerical results clearly show the qualitatively new behavior of the linear Cosserat model for our relaxed conformal curvature energy expression, case3. In contrast to the pointwise positive definite curvature energy (case1) and the symmetric case2 our relaxed energy provides a completely different spectrum of size-dependent behavior. This is what we expected on theoretical reasons [73] but which is also neatly covered by our numerical experiments.

In order to validate our simulations, we run first the linear elastic Cauchy response, which is included in the Cosserat model by setting $\mu_c > 0$ and $L_c = 0$. Then we slightly increase $L_c > 0$ to still observe comparable qualitative response. We have compared the results for the torque computation also with the results of Münch [71]. Since [71] is set up entirely in terms of geometrically exact expressions, we use, for comparison purposes only a nonlinear evaluation formula for the

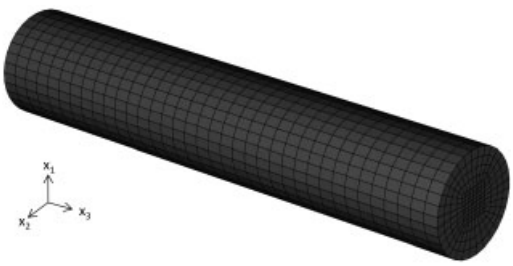

Number of elements	Type of elements	DOFs
6912	Hexahedral	198 618

Fig. 3 Mesh density illustration and mesh statistics for considered circular bar (Fig. 6).

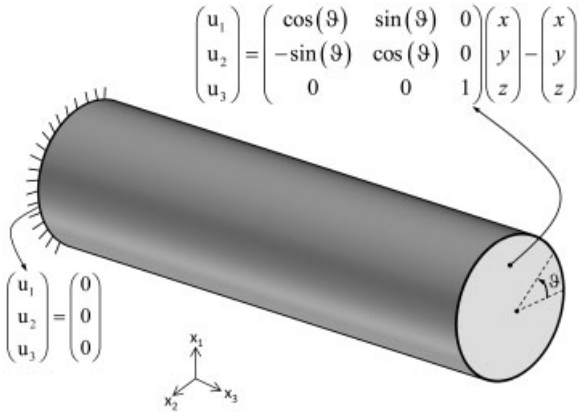

Fig. 4 Boundary conditions for the circular bar, clamped at the bottom and rotated at the top of cylinder by an exact rotation with angle ϑ.

stresses and an adapted application of boundary conditions in order to get as close as possible from our linear model to the geometrically exact development. This procedure is detailed in the appendix.

The torsion problem which we are going to consider gives rise to an inhomogeneous deformation field which makes it a fundamental test for each Cosserat model, small strain or finite strain. This holds since the Cosserat curvature expression is invariably activated. Despite the fact that we deal with a linear Cosserat model we **apply an exact rotation** at the upper face (at height L) of the sample with angle ϑ given by

$$\begin{pmatrix} \cos\vartheta & \sin\vartheta & 0 \\ -\sin\vartheta & \cos\vartheta & 0 \\ 0 & 0 & 1 \end{pmatrix} = \mathbb{1} + \begin{pmatrix} 0 & \vartheta & 0 \\ -\vartheta & 0 & 0 \\ 0 & 0 & 0 \end{pmatrix} + \dots . \tag{3.1}$$

3.2 Analytical torsion solution for circular cross-section without warping and linear boundary condition

If in the torsion problem the sample has circular cross-section with diameter $D = 2\,r$ and height L, then an analytical solution for the classical linear Cauchy-elastic problem is available which connects the rotation at the upper face with the applied angle. In this special case, the cross-sections remain plane (no warping) and each cross section is rotated along the torsion axis. Since we deal with a linear problem, the rotation angle in height z along the torsion axis is proportional to z. In terms of the deformation we have the Dirichlet boundary condition at the upper face

$$\varphi_L(x,y,L) = \begin{pmatrix} x \\ y \\ L \end{pmatrix} + \begin{pmatrix} 0 & \vartheta & 0 \\ -\vartheta & 0 & 0 \\ 0 & 0 & 0 \end{pmatrix} \begin{pmatrix} x \\ y \\ L \end{pmatrix}, \quad \text{Dirichlet boundary condition at upper face},$$

$$\varphi(x,y,z) = \begin{pmatrix} x \\ y \\ z \end{pmatrix} + \begin{pmatrix} \frac{\vartheta}{L}\, y\, z \\ -\frac{\vartheta}{L}\, x\, z \\ 0 \end{pmatrix}, \quad \text{deformation solution}. \tag{3.2}$$

It is simple to see that the Dirichlet boundary conditions $\varphi(x,y,0) = (x,y,0)$ (fixed at the bottom) and $\varphi(x,y,L) = \varphi_L(x,y,L)$ (infinitesimally rotated at upper face) are satisfied. Moreover, φ satisfies the linear elasticity equations. Therefore we get for the displacement

$$u(x,y,z) = \begin{pmatrix} \frac{\vartheta}{L}\, y\, z \\ -\frac{\vartheta}{L}\, x\, z \\ 0 \end{pmatrix}, \ \nabla u = \begin{pmatrix} 0 & \frac{\vartheta}{L}\, z & \frac{\vartheta}{L}\, y \\ -\frac{\vartheta}{L}\, z & 0 & -\frac{\vartheta}{L}\, x \\ 0 & 0 & 0 \end{pmatrix}, \ \operatorname{skew} \nabla u = \begin{pmatrix} 0 & \frac{\vartheta}{L}\, z & \frac{\vartheta}{2\,L}\, y \\ -\frac{\vartheta}{L}\, z & 0 & -\frac{\vartheta}{2\,L}\, x \\ -\frac{\vartheta}{2\,L}\, y & \frac{\vartheta}{2\,L}\, x & 0 \end{pmatrix},$$

$$\operatorname{sym} \nabla u = \begin{pmatrix} 0 & 0 & \frac{\vartheta}{2\,L}\, y \\ 0 & 0 & -\frac{\vartheta}{2\,L}\, x \\ \frac{\vartheta}{2\,L}\, y & -\frac{\vartheta}{2\,L}\, x & 0 \end{pmatrix}. \tag{3.3}$$

For very small angles ϑ we may compare this (completely linear)[6] solution against our FEM solution which has been calculated on the basis of (3.1).

The finite element analyses are performed for two different DOFs, i.e., 50000 DOFs and 200000 DOFs. Using **displacement Dirichlet boundary conditions** at the upper face of the cylindrical bar allows us to apply the geometrically exact angles even for large rotation angles. The relative error obtained via FEM are very small and show that the numerical and analytical results for small rotation angles match perfectly. Note again that microrotations remain free at the boundary.

For given applied rotation angle ϑ at the upper face we have

$$M_T = \frac{G\, I_T}{L}\, \vartheta\,, \quad I_T = \frac{\pi}{2}\, r^4 = \frac{\pi\, D^4}{32}\,, \quad G = \mu = \frac{E}{2\,(1+\nu)}\,. \tag{3.4}$$

Here, M_T is the applied torque, I_T is the torsion coefficient (here the polar moment of inertia) and $G = \mu\ (N/\mathrm{mm}^2)$ is the shear modulus. The torque about the e_3-axis at the upper surface $\partial\Omega^+$ is given by the following classical formula

$$M_T^{\mathrm{lin}} = \int_{\partial\Omega^+} (x\, \sigma_{32}^{\mathrm{lin}} - y\, \sigma_{31}^{\mathrm{lin}})\, \mathrm{d}x\, \mathrm{d}y = \mu\, \frac{\vartheta}{L} \int_{\partial\Omega^+} (x^2 + y^2)\, \mathrm{d}x\, \mathrm{d}y = \mu\, \frac{\vartheta}{L}\, I_T\,, \tag{3.5}$$

where we have used σ^{lin} according to (3.3). Note that in the micropolar model the total torque at the upper surface consists of this part and an integrated contribution coming from m_{33}. However, we have applied Neumann boundary conditions for the microrotation which implies $m_{33} = 0$.

Further, the applied torque based on the obtained exact Cauchy stresses (6.6) will be defined as follows

$$M_T^{\mathrm{exact}} = \int_{\partial\Omega^+} (x\, \sigma_{32}^{\mathrm{exact}} - y\, \sigma_{31}^{\mathrm{exact}})\, \mathrm{d}x\, \mathrm{d}y\,. \tag{3.6}$$

In the present paper, we obtain the torque value by integration on the upper surface of the cylindrical bar using (3.6) for the applied angles ($0 \le \vartheta \le (20\pi/180\,\mathrm{rad})$. The torque-torsion angle curve is plotted in Fig. 5. As illustrated in Fig. 5, the analytical solution differs from the calculated solution for larger torsion angles.

4 Checking two limit cases

We check next various other limiting cases, where the analytical solution can be read off at once.

4.1 Limit case: Cauchy elasticity in linear Cosserat elasticity

It is easy to see that one obtains the linear elasticity displacement solution for $\mu_c = 0$ and $L_c > 0$ in case1 since the system of equations decouples. For large L_c the microrotations approach a constant value over the entire body if there are no boundary conditions imposed on the microrotations. The system reads

$$\sigma = 2\mu \cdot \operatorname{sym} \overline{\varepsilon} + \lambda \cdot \operatorname{tr} [\overline{\varepsilon}] \cdot 1\!\!1\,, \quad m = \gamma \nabla \phi = \mu\, L_c^2 \nabla \phi\,, \tag{4.1}$$

$$\operatorname{Div} \sigma = 0\,, \quad \operatorname{Div} m = 0\,. \tag{4.2}$$

[6] In the linear analytical solution the boundary condition is applied linearly in ϑ. All our simulations are based, however, on prescribing exact rotations at the upper face. There, both $\cos\vartheta$ and $\sin\vartheta$ are used.

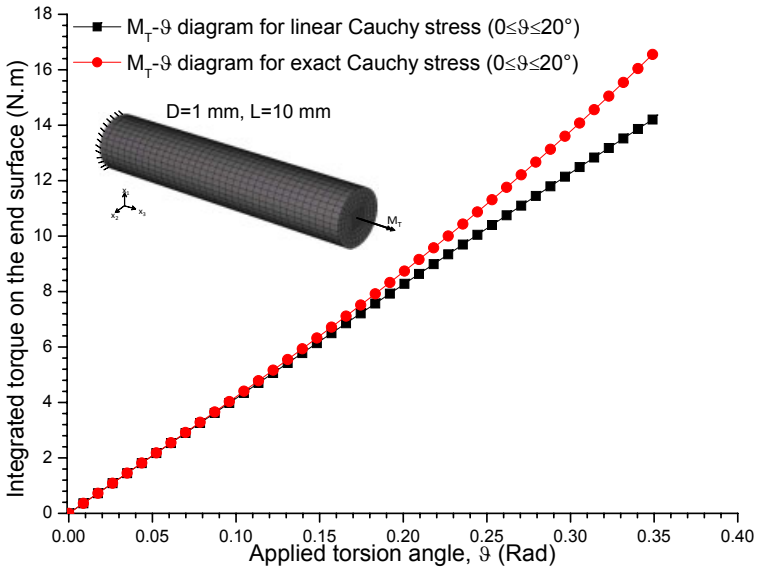

Fig. 5 (online colour at: www.zamm-journal.org) Torque-torsion angle diagram for the geometrically exact Cauchy stress and linear Cauchy stress ($0 \leq \vartheta \leq 20°$). Calculation based on Cosserat kinematics with $\mu_c > 0$ and $L_c = 0$. Note that $L_c = 0$ reduces the Cosserat model to classical Cauchy elasticity, which allows us to check our Cosserat algorithm against the classical torsion solution.

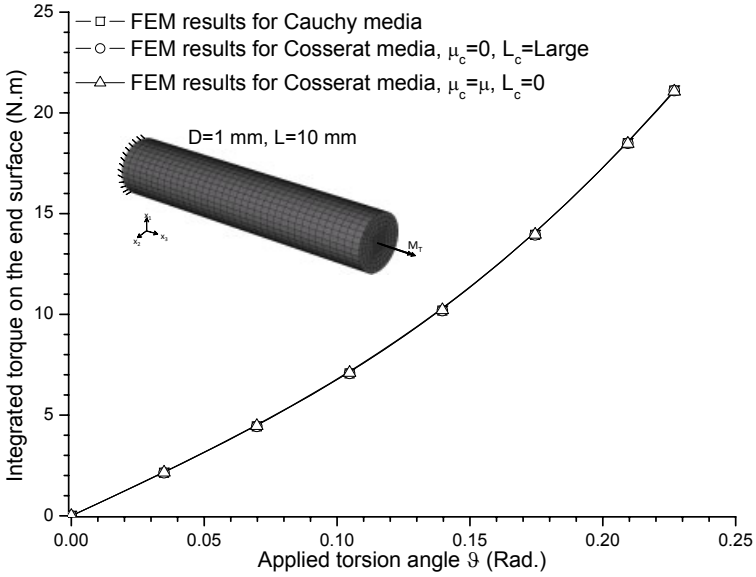

Fig. 6 Comparison among the Cauchy media, Cosserat case limit 1 ($\mu_c = 0$, L_c=Large) and Cosserat case limit 2 ($\mu_c = \mu$, $L_c = 0$) for $0 \leq \vartheta \leq 13°$. Calculation based on Cosserat kinematics.

A second alternative is to take $\mu_c = \mu$ and $L_c = 0$ which, in fact, also represents the linear elasticity solution. Since curvature is absent, the balance of angular momentum equation reduces to the pointwise equation $\operatorname{skew} \nabla u = \overline{A}$. Thus the skew-symmetric parts in the balance of force equation cancel and the displacement u is again the Cauchy displacement. In this work, we evaluate these two limit cases by considering $L_c = 1 \times 10^6$ mm and $\mu_c = 0$ for the first case to be sufficiently large in Linear Cosserat (case1) by FEM analysis and it is presented in Fig. 6 against the obtained Cauchy solution of the applied identical torsion with the same number of DOFs (DOFs=198618), which nearly presents only 0.14 percent of error. Our numerical results show that our implementation of the Cosserat model perfectly reproduces the linear elastic solution as limit cases of Cosserat elasticity.

4.2 Limit case: Constant infinitesimal mean rotation

Another (more difficult) limit case is $\mu_c > 0$ and $L_c = \infty$ with pointwise positive curvature, case1 in our curvature classification.[7] From the variational statement of the problem it is clear that the microrotation $\overline{A}$ must be a constant $\widehat{A} \in \mathfrak{so}(3)$ since the energy remains bounded. Minimizing the remaining energy therefore with respect to **constant microrotations** $\widehat{A}$

[7] In principle the same calculations can be done for conformal curvature. In this case we would be led to consider a ten-dimensional minimization problem for the parameters of the conformal map.

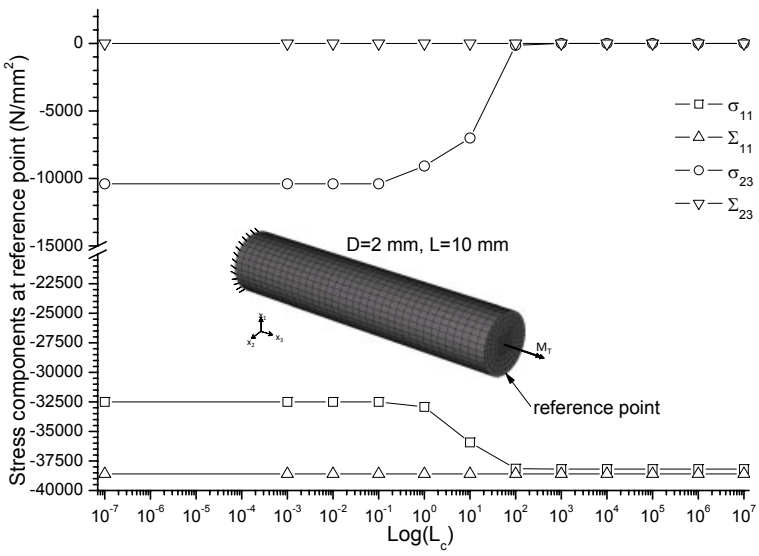

Fig. 7 Comparison between the limit solution of constant microrotation, formally $L_c = \infty$ and the Cosserat solution for large L_c.

leads to the problem

$$\int_\Omega \mu \,\|\operatorname{sym}\nabla u\|^2 + \mu_c \,\|\operatorname{skew}\nabla u - \widehat{A}\|^2 + \frac{\lambda}{2}\operatorname{tr}[\nabla u]^2 \,\mathrm{dV} \mapsto \min\,. \quad (u, \widehat{A})\,. \tag{4.3}$$

Thus the equilibrium equation for the constant $\widehat{A} \in \mathfrak{so}(3)$ reads

$$\begin{aligned} &\int_\Omega 2\mu_c \,\langle \operatorname{skew}\nabla u(x) - \widehat{A}, \delta\widehat{A}\rangle \,\mathrm{dV} = 0 \quad \forall \quad \delta\widehat{A} \in \mathfrak{so}(3) \quad \Rightarrow \\ &\langle \int_\Omega [\operatorname{skew}\nabla u(x) - \widehat{A}]\,\mathrm{dV}, \delta\widehat{A}\rangle = 0 \quad \forall \quad \delta\widehat{A} \in \mathfrak{so}(3) \quad \Rightarrow \\ &\int_\Omega \operatorname{skew}\nabla u(x)\,\mathrm{dV} = \int_\Omega \widehat{A}\,\mathrm{dV} = |\Omega|\,\widehat{A}\,. \end{aligned} \tag{4.4}$$

Therefore, the constant microrotation must have the value

$$\widehat{A} = \frac{1}{|\Omega|}\int_\Omega \operatorname{skew}\nabla u\,\mathrm{dV} = \operatorname{skew}\left[\frac{1}{|\Omega|}\int_\Omega \nabla u\,\mathrm{dV}\right] = \operatorname{skew}\left[\frac{1}{|\Omega|}\int_{\partial\Omega} u \otimes \vec{n}\,\mathrm{dS}\right]\,. \tag{4.5}$$

Thus the weak problem for the displacement reads then

$$\begin{aligned} 0 = \operatorname{Div}\sigma &= \operatorname{Div}\left[2\mu\operatorname{sym}\nabla u + 2\mu_c\operatorname{skew}(\nabla u - \widehat{A}) + \lambda\operatorname{tr}[\nabla u]\,1\!\!1\right] \\ &= \operatorname{Div}\left[2\mu\operatorname{sym}\nabla u + 2\mu_c\operatorname{skew}(\nabla u) + \lambda\operatorname{tr}[\nabla u]\,1\!\!1\right]\,, \end{aligned} \tag{4.6}$$

since $\widehat{A}$ is constant. Hence, once this equation is solved for the torsion-geometry, the stresses σ follow as

$$\sigma = 2\mu\,\operatorname{sym}\nabla u + 2\mu_c\operatorname{skew}(\nabla u - \widehat{A}) + \lambda\operatorname{tr}[\nabla u]1\!\!1\,. \tag{4.7}$$

Note that such a formulation is still infinitesimally frame-indifferent because the constant mean rotation filters out the infinitesimal rigid rotation. See Fig. 7 for a comparison between this solution and the Cosserat solution for large L_c.

5 Parameter study of linear Cosserat elasticity

We are now discussing the simulated response for the linear Cosserat elasticity model. The geometry and the boundary conditions remain the same as previously illustrated in Fig. 2. The mesh density and mesh statistics are displayed in Fig. 3. We use the exact rotation Dirichlet boundary conditions or so called essential boundary condition as given by (cf. Fig. 4):

$$\begin{aligned} &u_1 = 0\,, u_2 = 0\,, u_3 = 0\,, \quad \text{at the bottom} \\ &u_1 = x\cos\vartheta + y\sin\vartheta - x\,, u_2 = -x\sin\vartheta + y\cos\vartheta - y\,, u_3 = 0\,, \quad \text{at the top}\,. \end{aligned} \tag{5.1}$$

Table 1 Material properties for Cosserat circular bar.

Cases	case1	case2	case3
Young's Modulus $[\mathrm{N/mm^2}]$	1×10^6	1×10^6	1×10^6
Poisson's ratio $[-]$	0.3	0.3	0.3
$\mu = \mu_c$ $[\mathrm{N/mm^2}]$	$\mathrm{ds}\,\frac{E}{2(1+\nu)}$	$\mathrm{ds}\,\frac{E}{2(1+\nu)}$	$\mathrm{ds}\,\frac{E}{2(1+\nu)}$
λ $[\mathrm{N/mm^2}]$	$\mathrm{ds}\,\frac{\nu E}{(1+\nu)(1-2\nu)}$	$\mathrm{ds}\,\frac{\nu E}{(1+\nu)(1-2\nu)}$	$\mathrm{ds}\,\frac{\nu E}{(1+\nu)(1-2\nu)}$
α $[\mathrm{N}]$	0	0	$-\,\mathrm{ds}\,\frac{\mu L_c^2}{3}$
β $[\mathrm{N}]$	0	$\mathrm{ds}\,\frac{\mu L_c^2}{2}$	$\mathrm{ds}\,\frac{\mu L_c^2}{2}$
γ $[\mathrm{N}]$	μL_c^2	$\mathrm{ds}\,\frac{\mu L_c^2}{2}$	$\mathrm{ds}\,\frac{\mu L_c^2}{2}$
$L_c\,[\mathrm{mm}]$	$0 \le L_c \le 10 \times 10^6$	$0 \le L_c \le 10 \times 10^6$	$0 \le L_c \le 10 \times 10^6$
Square coupling number, N^2 $[-]$	$\mathrm{ds}\,\frac{1}{2}$	$\mathrm{ds}\,\frac{1}{2}$	$\mathrm{ds}\,\frac{1}{2}$
Polar ratio, Ψ $[-]$	1	1	$\mathrm{ds}\,\frac{3}{2}$

Remember that microrotations $\overline{A} \in \mathfrak{so}(3)$ are not constraint at the boundary, implying the free Neumann condition $m.\vec{n}_{|\partial\Omega} = 0$. The material parameters for our computations[8] are given in Table 1. The internal length scale parameter L_c will vary from very small values (nearly zero) to very high values (10×10^6 mm). Since the coupling between microrotations and displacements involves the term $\|\operatorname{curl} u - 2\operatorname{axl}(\overline{A})\|^2$, quadratic elements for u and linear interpolation for $\overline{A}$ have been used in our FEM approach. All computations have been carried out with 198618 DOFs (Fig. 3). The results are presented in Figs. 8–10.

5.1 Pointwise positive case1

We recall here the applied material parameters in curvature energy for this cases: $(\mu L_c^2/2)\|\nabla\phi\|^2$. This corresponds to $\alpha = 0$, $\beta = 0$, $\gamma = \mu L_c^2$ and the corresponding coupled system of equations is

$$\operatorname{Div}\sigma = 0\,, \quad \sigma = 2\mu\ \operatorname{sym}(\nabla u - \overline{A}) + 2\mu_c\ \operatorname{skew}(\nabla u - \overline{A}) + \lambda \operatorname{tr}[\overline{\varepsilon}]\cdot \mathbb{1}\,, \tag{5.2}$$

$$\operatorname{Div} m + 4\mu_c \cdot \operatorname{axl}\operatorname{skew}\overline{\varepsilon} = 0\,, \quad m = \mu L_c^2 \nabla\phi\,. \tag{5.3}$$

We apply the exact angle ϑ on the top from 0 to $\frac{13\pi}{180}$(rad) for each value of L_c which is varied from zero to 10×10^6 mm. The numerical solution for linear Cosserat elasticity with pointwise positive curvature exhibits more stiffness for higher values of L_c in an asymptotic manner (Fig. 8). We observe a bound on the stiffness (the tangent in the plot) for L_c values greater than 100 mm (Fig. 8). Case1 reveals significantly more stiffening effects than the other cases (Fig. 9 and Fig. 10).

5.2 Symmetric case2

The curvature form in Cosserat linear elasticity in this cases is : $\frac{\mu L_c^2}{2}\|\operatorname{sym}\nabla\phi\|^2$ and the moment stress tensor m is also symmetric. The corresponding material parameters are $\alpha = 0$, $\beta = \gamma = \frac{\mu L_c^2}{2}$ and the coupled system of equations is

$$\operatorname{Div}\sigma = 0\,, \quad \sigma = 2\mu \cdot \operatorname{sym}(\nabla u - \overline{A}) + 2\mu_c \cdot \operatorname{skew}(\nabla u - \overline{A}) + \lambda \operatorname{tr}[\overline{\varepsilon}]\cdot \mathbb{1}\,, \tag{5.4}$$

$$\operatorname{Div} m + 4\mu_c \cdot \operatorname{axl}\operatorname{skew}\overline{\varepsilon} = 0\,, \quad m = \mu L_c^2 \cdot \operatorname{sym}\nabla\phi\,. \tag{5.5}$$

The numerical solution for the linear Cosserat elasticity with symmetric positive curvature exhibits more stiffness for higher values of L_c by an asymptotic manner (Fig. 9) as seen before. We observe a bound on the stiffness for L_c values greater than 100 mm (Fig. 9).

[8] It is well worth mentioning that the modulus of elasticity in Table 1 deals with diamond. Diamond is a most unlikely choice as a Cosserat material. In the present paper, we have chosen this value only for the numerical experiments.

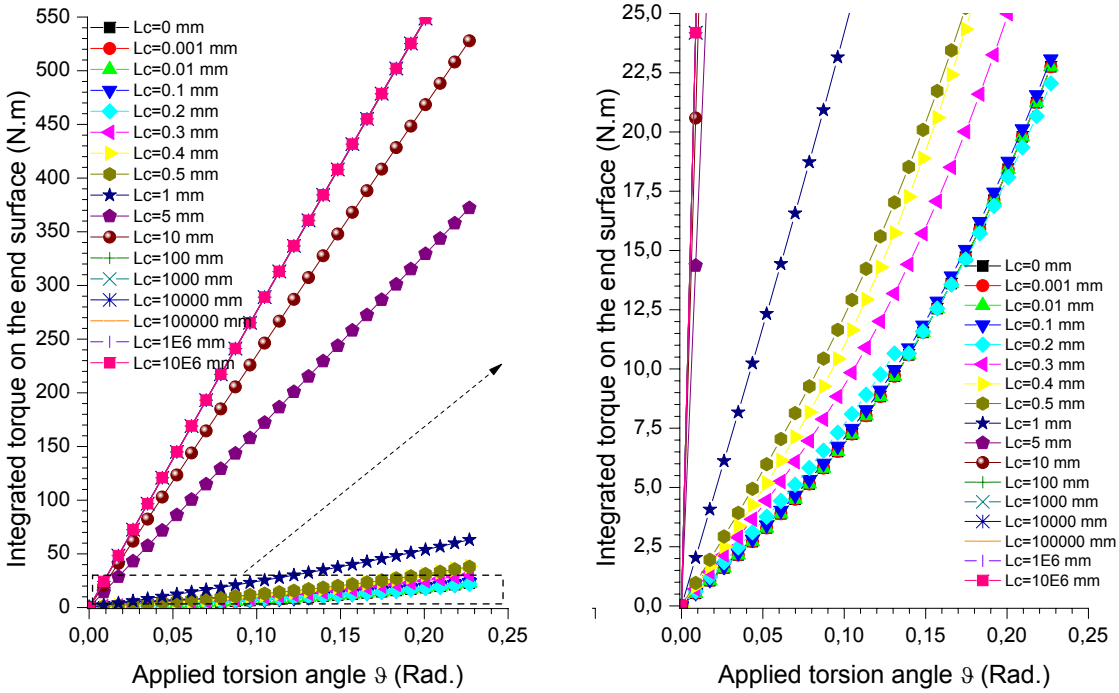

Fig. 8 (online colour at: www.zamm-journal.org) Results for fixed $\mu = \mu_c$ and variation of L_c[mm] for pointwise positive curvature ($D = 2\,\text{mm},\ L = 10\,\text{mm}$).

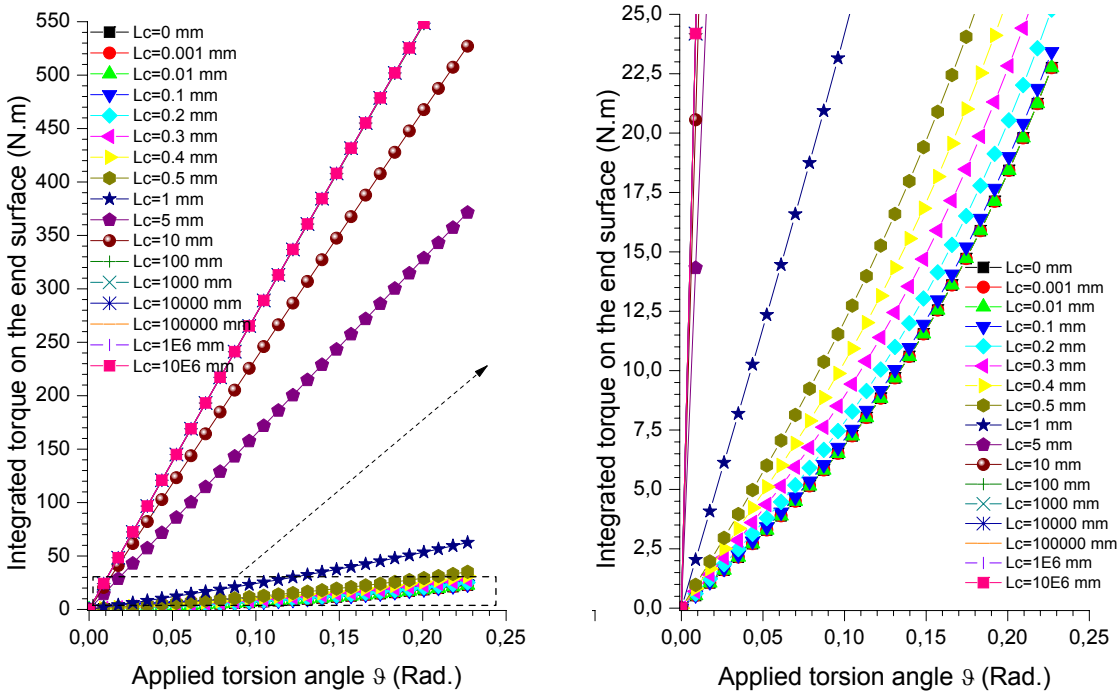

Fig. 9 (online colour at: www.zamm-journal.org) Results for fixed $\mu = \mu_c$ and variation of L_c[mm] for symmetric curvature ($D = 2\,\text{mm},\ L = 10\,\text{mm}$).

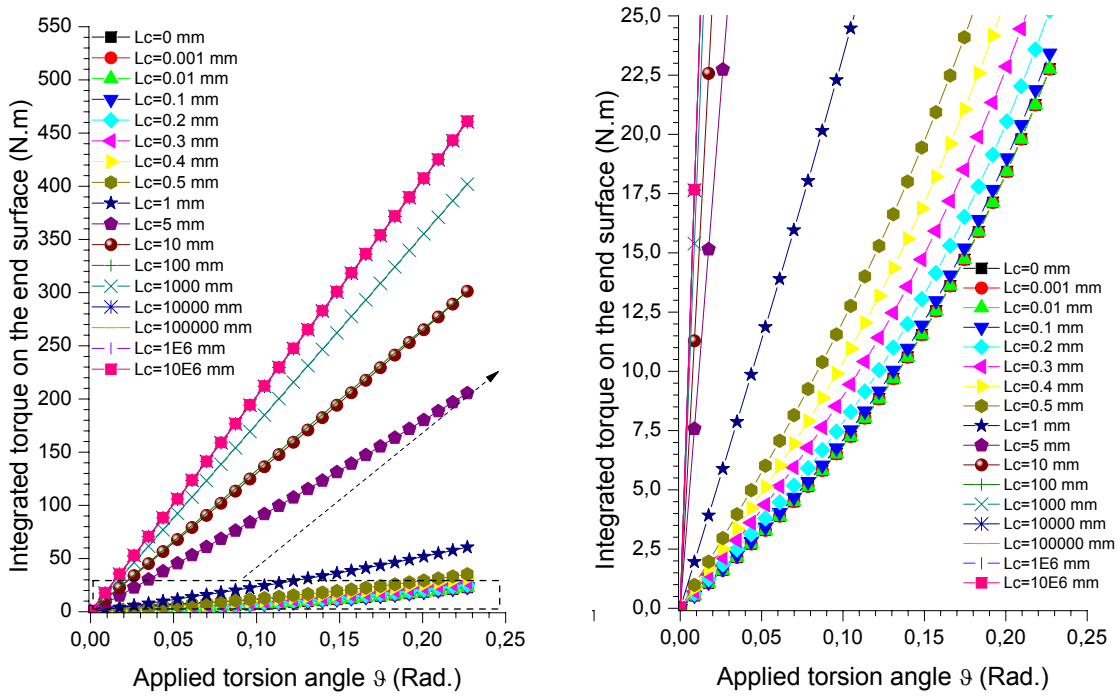

Fig. 10 (online colour at: www.zamm-journal.org) First results for fixed $\mu = \mu_c$ and variation of L_c[mm] for conformal curvature.

5.3 Conformal case3

We recall here the relaxed curvature energy in this cases: $(\mu L_c^2/2)\|\operatorname{dev}\operatorname{sym}\nabla\phi\|^2$. This leads to $\alpha = (-1/3)\mu\, L_c^2$, $\beta = \gamma$, $\gamma = \mu\, L_c^2$ as parameters. The moment stress tensor m is symmetric and trace-free and the corresponding coupled system of equations reads

$$\operatorname{Div}\sigma = 0\,, \quad \sigma = 2\mu\cdot\operatorname{sym}(\nabla u - \overline{A}) + 2\mu_c\cdot\operatorname{skew}(\nabla u - \overline{A}) + \lambda\operatorname{tr}[\overline{\varepsilon}]\cdot 1\!\!1\,, \tag{5.6}$$

$$\operatorname{Div} m + 4\,\mu_c\cdot\operatorname{axl}\operatorname{skew}\overline{\varepsilon} = 0\,, \qquad m = \mu L_c^2\left(\operatorname{sym}\nabla\phi - \frac{1}{3}\operatorname{tr}[\nabla\phi]\cdot 1\!\!1\right)\,. \tag{5.7}$$

The numerical solution for the linear Cosserat elasticity with conformal positive curvature displays again more stiffness for higher values of L_c (Fig. 10) and we observe a bound on the stiffness for L_c values now greater than 1000 mm (Fig. 10).

5.4 Torque – Log diagram

According to the last results it is possible to plot the torque magnitude at the top of the cylindrical bar versus "Log(L_c)" in a semi-logarithmic diagram (Fig. 11) for a given torsion angle ϑ. In Fig. 11, we chose ϑ equal to $13°$ ($\vartheta = 13\pi/180$ rad) and we plot the Torque-Log(L_c) diagram for all cases (case1, case2, and case3). Evidently, we find the upper and lower bound for the stiffness M_T. In the diagram we distinguish three specific zones: **Zone I** tends toward linear Cauchy elasticity with no size effects present, **Zone II** is an intermediate zone in which the size effects appear and we can clearly distinguish the Cosserat effects for our numerical models, **Zone III** describes a situation where the microrotation is nearly constant with the limit behavior discussed explicitly in Sect. 4.2. The most interesting zone is the intermediate Zone II. We see that the pattern given for case1 and case2 has been disturbed beyond Zone I in case3 and only later it gets the expected pattern (Fig. 12). This distinguishing phenomenon for case3 means less stiffening effects and a more pronounced size effect (the spread between linear elasticity and constant mean rotation, i.e. where size-dependent response occurs, it covers orders of magnitude for larger L_c-values).

The case1 and case2 show practically the same behavior in this Torque-Log(L_c) diagram, whereas case3 behaves in a completely different manner! This is due to the fact that we have the third constitutive parameter ($\alpha = -(\mu L_c^2/3) < 0$) for the couple stress-curvature tensor constitutive law. The Torque-Log diagram Fig. 11 indicates a completely different size-effect response for the conformal case. It can be seen that in the conformal case a much larger L_c-value can be taken to produce the same amount of torque at equal applied rotation angle ϑ. Thus, in an inverse calculation for the determination

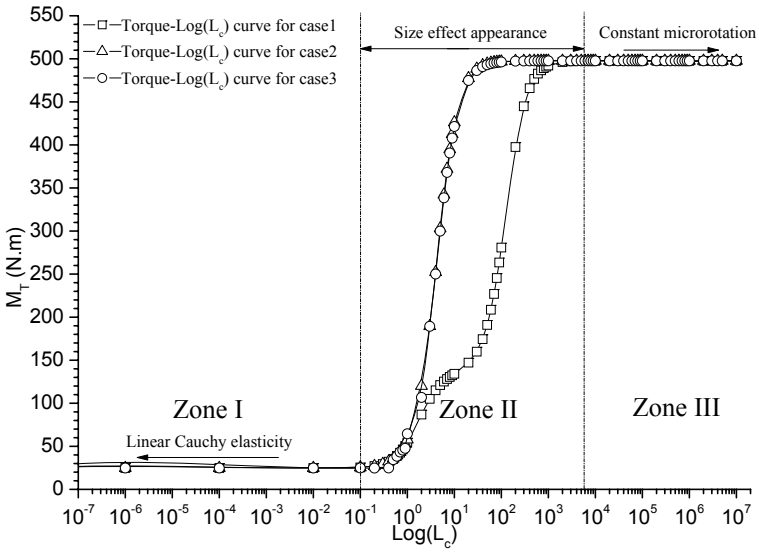

Fig. 11 Torque versus L_c in a semi-logarithmic diagram ($M_T - Log(L_c)$) for the cylindrical bar (L = 10 mm and D = 2 mm) and $\vartheta = 13^\circ = 13\pi/180$ rad.

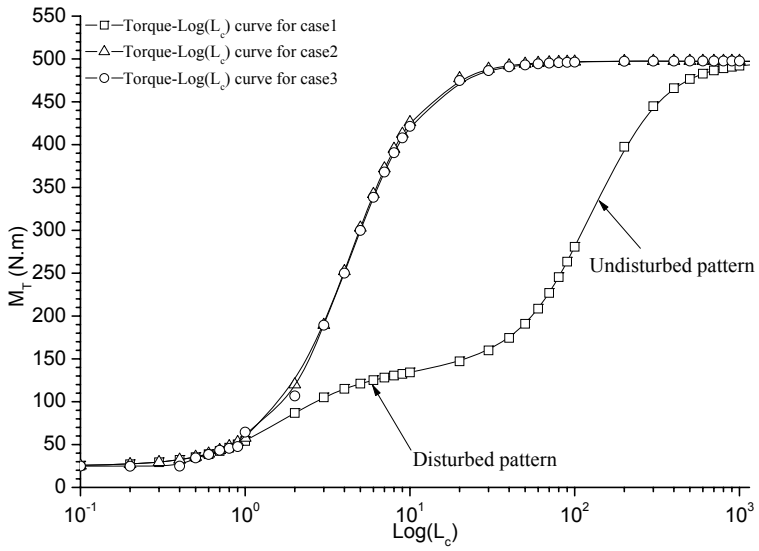

Fig. 12 **Zone II** of $M_T - Log(L_c)$ diagram for the cylindrical bar (L = 10 mm and D = 2 mm) and $\vartheta = 13^\circ = 13\pi/180$ rad.

of the characteristic size (related to L_c), we may obtain these larger L_c-values. Note that a typical problem in the parameter-fitting of Cosserat models based on case1 or case2 is that the fitted L_c-values would be orders of magnitude smaller than anything which could physically serve as setting a characteristic size. This can be circumvented in the conformal case.

From our numerical experiments we observe that case2 and case3 are numerically more stable than case1 in the sense that better convergence rates have always been observed with a consistent runtime reduction. Surprisingly, for case1, at the beginning of Zone II, we have observed some numerical instabilities (in the range $0.5\,\text{mm} \leq L_c \leq 0.75\,\text{mm}$).

The aforementioned semi-logarithmic diagram rises some questions about the nature of L_c and its role in the size effects phenomenon for the Cosserat media. Furthermore, the characteristic length much greater than cylinder size can be considered hardly physical and has never been experimentally realized [21]. Indeed, L_c can be implicitly interpreted as a phenomenological parameter which was originally proposed by Toupin in the early sixties [81]. According to the Toupin's study, L_c was nothing else than square root of γ over μ and it was developed in several directions for different applications by Gauthier [82–84] [9], Forest et al. [32, 34], and Alsaleh et al. [85–87]. In fact, the stiffness over curvature stiffness ratio determines whether one material has size effect behavior or not and L_c can be deemed as a parameter which handles it. Hence, very small L_c values treat classical Cauchy's media (the specimen geometry is several times bigger than so-called microstructure) and very high L_c values means that the specimen geometry is several times smaller than the microstructure.

[9] The Gauthier's analytical solution for the pure torsion test establish a benchmark tool for determining the Cosserat moduli. As for the comparison with Gauthier's exact solution, if the rod is sufficiently long, differences in the details of the end condition will fade out according to the Saint-Vennat's principle. It is of great importance to remind that the Dirichlet boundary conditions or so called essential boundary conditions drastically change the analytical solution form. This fact can be clearly observed in the analytical solution of the long torsion test. In the other cases, the finite element analyses provide more beneficial outcomes.

The middle zone (Zone II) represents a state in which the specimen geometry and so-called microstructure are in the same order of magnitude.

The main objective is to converge two different points of view. In the Lakes paper [21], the specimen geometry is experimentally reduced to obtain the size effects and two length scales have been extracted, whereas, herein, we did not change the specimen geometry in our numerical studies and we have changed the length scale L_c values for finding out the size effects (case1, 2, and 3).

As indicated before, the numerical simulation of Cosserat solids traditionally uses case 1 ($\alpha = \beta = 0$ and $\gamma = \mu L_c^2$) [16,42,43,88] and particular case of case1 or so called deviatoric case1 ($\alpha = \beta = 0$ and $\gamma = (\mu L_c^2/2)$) [73,89]. Case2 has been also applied to the Cosserat solids ([34,63,64,90]). In the previous work [73] and the present paper, we have evoked three possible choices for the form of curvature energy. Each considered form of energy has been investigated based upon the mathematical aspects [48,73]. Therefore, we have found out these choices as the possible forms of energy. However, we are not after a physical meaningful simulation of a real Cosserat material in the present paper, but we want to explore the possible parameter ranges.

6 Discussion

The reduction in Cosserat parameters from six to four in the 3D-case which is embodied in the conformal case3 can also be motivated from the physical principle of bounded stiffness for very small samples and the use of the analytical solution formulas for these cases, see the detailed discussion in [48,73]. It remains to be investigated whether conformal invariance is, in fact, a more primitive physical concept, perhaps to be motivated by novel invariance principles, with consequences for the Cosserat model. Here, we have shown that the novel conformal model allows for a numerical treatment and is therefore ready to use in practical applications. By comparing it with the more standard Cosserat approach (case1) we have demonstrated that the novel conformal model (case3) still shows a size-effect, which is, however, completely different than the traditional one with pointwise positive curvature (case1) or symmetric curvature (case2) of our classification. It allows for dramatically increased values of the internal length scale L_c still giving us a size effect in torsion and not constraining the microrotation to be constant over the sample for larger L_c-values.

We think that the conformal curvature expression offers therefore a fresh departure for the experimental determination of the remaining two Cosserat constants: one coupling constant μ_c and only one internal length scale L_c. We hope that other groups will take up this route as well and provide physically consistent parameter values for the linear Cosserat model for specific materials.

Acknowledgements The authors gratefully acknowledge anonymous reviewers for their valuable suggestions and comments to improve the quality of the paper.

Appendix: Geometrically exact application of torsion angle

For comparison purposes with our own nonlinear calculations [71], we propose a nonstandard representation of the stresses which will be as far as possible be consistent with geometrically exact strain measures, only the first Piola-Kirchhoff stresses S_1 will derive from a quadratic potential $W(F)$, thus ultimately destroying geometrical exactness.

Let us summarize the necessary relations. The first Piola-Kirchhoff stresses in nonlinear elasticity are given by

$$S_1(F) = D_F W(F) = \det[F]\, \sigma^{\text{exact}}\, F^{-T}\,, \tag{6.1}$$

where $F = \nabla\varphi = 1\!\!1 + \nabla u$ is the deformation gradient and ∇u the displacement gradient and the exact Cauchy stress σ^{exact} follows as usual from (6.1)

$$\sigma^{\text{exact}}(F) = \frac{1}{\det[F]}\, S_1(F)\, F^T\,. \tag{6.2}$$

The same definitions apply, with appropriate changes, also to the Cosserat model. Thus we have two possibilities to calculate the stresses either according to the linear Cosserat model or by linear Cauchy elasticity.

Recalling the energy contributions (W_{mp} for Cosserat linear elasticity and W_{lin} for classical linear elasticity) giving rise to the classical stresses, we have

$$W_{\text{mp}}(\overline{\varepsilon}) = \mu \|\operatorname{sym}\overline{\varepsilon}\|^2 + \mu_c \|\operatorname{skew}\overline{\varepsilon}\|^2 + \frac{\lambda}{2}\operatorname{tr}[\overline{\varepsilon}]^2\,, \qquad W_{\text{lin}}(\varepsilon) = \mu\,\|\varepsilon\|^2 + \frac{\lambda}{2}\operatorname{tr}[\varepsilon]^2\,, \tag{6.3}$$

where the applied kinematic relation for each case is:

$$\overline{\varepsilon} = \nabla u - \overline{A} = F - \mathbb{1} - \overline{A}\,, \qquad \varepsilon = \operatorname{sym} \nabla u = \operatorname{sym}(F - \mathbb{1})\,. \tag{6.4}$$

This leads to the respective first Piola-Kirchhoff stresses S_1^{mp} for Cosserat linear elasticity and S_1^{lin} for classical linear elasticity, i.e.,

$$\begin{aligned} S_1^{\mathrm{mp}}(F,\overline{A}) =& D_F W_{\mathrm{mp}}(F,\overline{A}) = 2\mu\,(\operatorname{sym} F - \mathbb{1} - \overline{A}) + 2\mu_c \operatorname{skew}(F - \mathbb{1} - \overline{A}) \\ &+ \lambda \operatorname{tr}\left[\operatorname{sym} F - \mathbb{1} - \overline{A}\right] \mathbb{1}\,, \\ S_1^{\mathrm{lin}}(F) =& D_F W_{\mathrm{lin}}(F) = 2\mu\,(\operatorname{sym} F - \mathbb{1}) + \lambda \operatorname{tr}\left[\operatorname{sym} F - \mathbb{1}\right] \mathbb{1}\,. \end{aligned} \tag{6.5}$$

Inserting $S_1^{\mathrm{lin}}(F)$ into the Cauchy stress formula (6.2) we obtain the Cauchy stresses in the actual configuration from

$$\begin{aligned} \sigma^{\mathrm{exact}}(F) &= \frac{1}{\det[F]}\, S_1^{\mathrm{lin}}(F)\, F^T = \frac{1}{\det[F]}\, \left(2\mu\,(\operatorname{sym} F - \mathbb{1}) + \lambda \operatorname{tr}\left[\operatorname{sym} F - \mathbb{1}\right] \mathbb{1}\ \right)\, F^T \\ &= \frac{1}{\det[\mathbb{1} + \nabla u]}\, \left(2\mu\,(\varepsilon + \lambda \operatorname{tr}\left[\varepsilon\right] \mathbb{1}\ \right)\, (\mathbb{1} + \nabla u)^T = \frac{1}{\det[\mathbb{1} + \nabla u]}\, \sigma^{\mathrm{lin}}(\varepsilon)\, (\mathbb{1} + \nabla u)^T\,, \end{aligned} \tag{6.6}$$

and similarly for S_1^{mp}. This formula for σ^{exact} will be used in the evaluation of the torque in (3.6).

References

[1] E. Cosserat and F. Cosserat, Théorie des corps déformables. (Librairie Scientifique A. Hermann et Fils (engl. translation by D. Delphenich 2007, pdf available at http://www.mathematik.tu-darmstadt.de/fbereiche/analysis/pde/staff/neff/patrizio/Cosserat.html), Paris, 1909).

[2] E. Cosserat and F. Cosserat, Note sur la théorie de l'action euclidienne, in: Traité de Mécanique Rationelle, edited by P. Appell (Gauthier-Villars, Paris, 1909), pp. 557–629.

[3] W. Günther, Zur Statik und Kinematik des Cosseratschen Kontinuums, Abh. Braunschweig Wiss. Ges. **10**, 195–213 (1958).

[4] R. Mindlin and H. Tiersten, Effects of couple stresses in linear elasticity, Arch. Rat. Mech. Anal. **11**, 415–447 (1962).

[5] R. Mindlin, Influence of couple-stresses on stress concentrations, Experimental Mechanics **3**(1), 1–7 (1963).

[6] R. Mindlin, Micro-structure in linear elasticity, Arch. Rat. Mech. Anal. **16**, 51–77 (1964).

[7] R. Mindlin, Second gradient of strain and surface tension in linear elasticity, Int. J. Solids Struct. **1**, 417–438 (1965).

[8] R. Mindlin and N. Eshel, On first strain-gradient theories in linear elasticity, Int. J. Solids Struct. **4**, 109–124 (1968).

[9] R. Mindlin, Theories of elastic continua and crystal lattice theories, in: Mechanics of Generalized Continua. Proceedings of the IUTAM-Symposium on the generalized Cosserat continuum and the continuum theory of dislocations with applications in Freudenstadt, 1967, edited by E. Kröner (Springer, 1968), pp. 312–320.

[10] A. Eringen and E. Suhubi, Nonlinear theory of simple micro-elastic solids, Int. J. Eng. Sci. **2**, 189–203 (1964).

[11] A. Eringen, Theory of micropolar fluids, J. Math. Mech. **16**, 1–18 (1966).

[12] A. Eringen, Theory of micropolar plates, Z. Angew. Math. Phys. **18**, 12–30 (1967).

[13] A. Eringen, Theory of Micropolar Elasticity, in: Fracture. An advanced treatise, edited by H. Liebowitz (Academic Press, New York, 1968), pp. 621–729.

[14] A. Eringen and C. Kafadar, Polar Field Theories, in: Continuum Physics, edited by A. Eringen (Academic Press, New York, 1976), pp. 1–73.

[15] A. Eringen, Theory of thermo-microstretch elastic solids, Int. J. Engng. Sci. **28**, 1291–1301 (1990).

[16] A. C. Eringen, Microcontinuum Field Theories (Springer, Heidelberg, 1999).

[17] S. Cowin, An incorrect inequality in micropolar elasticity theory, Z. Angew. Math. Physik **21**, 494–497 (1970).

[18] A. Yavari, S. Sarkani, and J. E. T. Moyer, On fractal cracks in micropolar elastic solids, J. App. Mech, ASME **69**(1), 45–59 (2002).

[19] R. S. Lakes, Cosserat micromechanics of human bone: strain redistribution by a hydration-sensitive constituent, J. Biomechanics **19**(5), 385–397 (1986).

[20] R. S. Lakes, S. Nakamura, J. Behiri, and W. Bonfield, Fracture mechanics of bone with short cracks, J. Biomechanics **23**(10), 967–975 (1990).

[21] R. S. Lakes, Experimental microelasticity of two porous solids, Int. J. Solids Struct. **22**(1), 55–63 (1986).

[22] H. Park and R. Lakes, Torsion of a micropolar elastic prism of square cross section, Int. J. Solids Struct. **23**, 485–503 (1987).

[23] R. S. Lakes, Experimental micro mechanics methods for conventional and negative poisson's ratio cellular solids as Cosserat continua, Journal of Mechanical Design **113**(1), 148–155 (1991).

[24] R. S. Lakes, Strongly Cosserat elastic lattice and foam materials for enhanced toughness, Cellular Polymers **12**(1), 17–30 (1993).

[25] W. Anderson and R. Lakes, Size effects due to Cosserat elasticity and surface damage in closed-cell polymethacrylimide foam, J. Mat. Sci. **29**, 6413–6419 (1994).

[26] C. Tekoglu, Size effect in cellular solids, PhD thesis, Rijksunivesiteit, Netherlands, 2007.

[27] G. Hu, X. Liu, and T. J. Lu, A variational method for non-linear micropolar composites, Mech. Mater. **37**, 407–425 (2005).
[28] P. Venna and D. Gastaldi, A voronoi cell finite element model for the identation of graded ceramic composites, Composite B **36**, 115–126 (2005).
[29] H. W. Zhang, H. Wang, and J. B. Wang, Parametric variational principle based elastic-plastic analysis of materials with polygonal and voronoi cell finite element methods, Finite Elem. Anal. Des. **43**(3), 206–217 (2007).
[30] H. Zhang, H. Wang, B. Chen, and Z. Xie, Analysis of Cosserat materials with voronoi cell finite element method and parametric variational principle, Comp. Meth. Appl. Mech. Engrg. **197**(6–8), 741–755 (2008).
[31] S. Forest, G. Cailletaud, and R. Sievert, A Cosserat theory for elastoviscoplastic single crystals at finite deformation, Arch. Mech. **49**(4), 705–736 (1997).
[32] R. Dendievel, S. Forest, and G. Canova, An estimation of overall properties of heterogeneous Cosserat materials, in: Mechanics of Materials with Intrinsic Length Scale: Physics, Experiments, Modelling and Applications, edited by A. Bertram and F. Sidoroff, Journal Physique IV France 8 (EDP Sciences, France, 1998), pp. 111–118.
[33] S. Forest, Mechanics of generalized continua: construction by homogenization, J. Phys. IV France **8**, Pr4–39–Pr4–48 (1998).
[34] S. Forest, R. Dendievel, and G. Canova, Estimating the overall properties of heterogeneous Cosserat materials, Modelling Simul. Mater. Sci. Eng. **7**, 829–840 (1999).
[35] S. Forest, An estimation of overall properties of heterogeneous Cosserat materials, in: Geometry, Continua and Microstructure, edited by G. MauginTravaux en Cours No. 60 (Hermann, Paris, France, 1999), pp. 35–48.
[36] S. Forest, F. Barbe, and G. Cailletaud, Cosserat modelling of size effects in the mechanical behaviour of polycrystals and multiphase materials, Int. J. Solids Struct. **37**, 7105–7126 (2000).
[37] S. Forest, Homogenization methods and the mechanics of generalized continua - Part 2, Theoret. Appl. Mech. (Belgrad) **28–29**, 113–143 (2002).
[38] S. Forest, R. Sievert, and E. Aifantis, Strain gradient crystal plasticity: thermodynamical formulations and applications, J. Mech. Beh. Mat. **13**, 219–232 (2002).
[39] S. Forest and R. Sievert, Nonlinear microstrain theories, Int. J. Solids Struct. **43**, 7224–7245 (2006).
[40] M. Ristinmaa and M. Vecchi, Use of couple-stress theory in elasto-plasticity, Comput. Meth. Appl. Mech. Engrg. **136**, 205–224 (1996).
[41] P. Neff, A finite-strain elastic-plastic Cosserat theory for polycrystals with grain rotations, Int. J. Eng. Sci. **44**, 574–594 (2006), DOI 10.1016/j.ijengsci.2006.04.002.
[42] P. Neff, K. Chełmiński, W. Müller, and C. Wieners, A numerical solution method for an infinitesimal elastic-plastic Cosserat model, Preprint 2470, http://www3.mathematik.tu-darmstadt.de/fb/mathe/bibliothek/preprints.html, Math. Mod. Meth. Appl. Sci. (M3AS) **17**(8), 1211–1239 (2007).
[43] P. Neff and S. Forest, A geometrically exact micromorphic model for elastic metallic foams accounting for affine microstructure. Modelling, existence of minimizers, identification of moduli and computational results, J. Elasticity **87**, 239–276 (2007).
[44] F. Vernerey, W. K. Liu, and B. Moran, Multi-scale micromorphic theory for hierarchical materials, J. Mech. Phys. Solids **55**(12), 2603–2651 (2007).
[45] F. J. Vernerey, W. K. Liu, B. Moran, and G. Olson, A micromorphic model for the multiple scale failure of heterogeneous materials, J. Mech. Phys. Solids **56**(4), 1320–1347 (2008).
[46] P. Neff, The Cosserat couple modulus for continuous solids is zero viz the linearized Cauchy-stress tensor is symmetric, Preprint 2409, http://www3.mathematik.tu-darmstadt.de/fb/mathe/bibliothek/preprints.html, Z. Angew. Math. Mech. **86**, 892–912 (2006).
[47] P. Neff, Existence of minimizers for a finite-strain micromorphic elastic solid, Preprint 2318, http://www3.mathematik.tu-darmstadt.de/fb/mathe/bibliothek/preprints.html, Proc. Roy. Soc. Edinb. A **136**, 997–1012 (2006).
[48] J. Jeong and P. Neff, Existence, uniqueness and stability in linear Cosserat elasticity for weakest curvature conditions, Mathematics and Mechanics of Solids (2008), First published on September 17, 2008, doi:10.1177/1081286508093581.
[49] S. K. M. Baluch and J. E. Goldberg., Finite element approach to plane microelasticity, J. Struct. Division-American Soc. Civil Eng. **98**, 1957–1964 (1972).
[50] R. L. S. Nakamura and R. Benedict, Finite element method for orthotropic micropolar elasticity, Int. J. Engrg. Sci. **22**, 319–330 (1984).
[51] E. Providas and M. Kattis, Finite element method in plane Cosserat elasticity, Comput. Struct. **80**, 2059–2069 (2002).
[52] P. Trovalusci and R. Masiani, Non-linear micropolar and classical continua for anisotropic discontinuous materials, Int. J. Solids Struct. **40**(5), 1281–1297 (2003).
[53] M. R. B. Nadler, A new 3-d finite element method for nonlinear elasticity using the theory of a Cosserat point, Int. J. Solids Struct. **40**, 4585–4614 (2003).
[54] C. Jog, Higher-order shell elements based on the Cosserat model, and their use in the topology design of strutures, Comput. Meth. Appl. Mech. Engrg. **193**, 2191–2220 (2004).
[55] L. Li and S. Xie, Finite element method for linear micropolar elasticity and numerical study of some scale effects phenomena in MEMS, Int. J. Mech. Sci. **46**, 1571–1587 (2004).
[56] S. Diebels and H. Steeb, The size effect in foams and its theoretical and numerical investigation, Proc. R. Soc. London A **458**, 2869–2883 (2002).
[57] S. Diebels and H. Steeb, Stress and couple stress in foams, Comput. Mat. Sci. **28**, 714–722 (2003).
[58] W. Ehlers, S. Diebels, and W. Volk, Deformation and compatibilty for elasto-plastic micropolar materials with applications to geomechanical problems, in: Mechanics of Materials with Intrinsic Length Scale: Physics, Experiments, Modelling and Applications, edited by A. Bertram and F. Sidoroff, Journal Physique IV France 8 (EDP Sciences, France, 1998), pp. 127–134.

[59] A. Dietsche, P. Steinmann, and K. Willam, Micropolar elastoplasticity and its role in localization, Int. J. Plasticity **9**, 813–831 (1993).
[60] E. Sharbati and R. Naghdabadi, Computational aspects of the Cosserat finite element analysis of localization phenomena, Comput. Mat. Sci. **38**, 303–315 (2006).
[61] P. Grammenoudis and C. Tsakmakis, Predictions of microtorsional experiments by micropolar plasticity, Proc. Roy. Soc. London A **461**, 189–205 (2005).
[62] F. Huang, B. Yan, J. Yan, and D. Yang, Bending analysis of micropolar elastic beam using a 3-d finite element method, Int. J. Engng. Sci. **38**, 275–286 (2000).
[63] B. Zastrau, Zur Berechnung orientierter Kontinua – Entwicklung einer Direktorentheorie und Anwendung der Finiten Elemente, No. 4/60 in Fortschrittberichte der VDI Zeitschriften (Verein Deutscher Ingenieure, VDI-Verlag GmbH, Düsseldorf, 1981).
[64] B. Zastrau and H. Rothert, Herleitung einer Direktortheorie für Kontinua mit lokalen Krümmungseigenschaften, Z. Angew. Math. Mech. **61**, 567–581 (1981).
[65] R. Stojanovic, On the mechanics of materials with microstructure, Acta Mech. **15**, 261–273 (1972).
[66] R. Rivlin, The formulation of theories in generalized continuum mechanics and their physical significance, Symp. Math. **1**, 357–373 (1969).
[67] F. Yang, A. Chong, D. Lam, and P. Tong, Couple stress based strain gradient theory for elasticity, Int. J. Solids Struct. **39**, 2731–2743 (2002).
[68] X. Li and H. Tang, A consistent return mapping algorithm for pressure-dependent elastoplastic Cosserat continua and modelling of strain localizaton, Comput. Struct. **83**(1), 1–10 (2005).
[69] A. Khoei, A. Tabarraie, and A. Gharehbaghi, H-adaptive mesh refinement for shear band localization in elasto-plasticity Cosserat continuum, Commun. Nonlinear Sci. Numer. Simul. **10**, 253–286 (2005).
[70] P. Grammenoudis and C. Tsakmakis, Finite element implementation of large deformation micropolar plasticity exhibiting isotropic and kinematic hardening effects, Int. J. Num. Meth. Engng. **62**(12), 1691–1720 (2005).
[71] I. Münch, Ein geometrisch und materiell nichtlineares Cosserat-Modell - Theorie, Numerik und Anwendungmöglichkeiten. (Dissertation in der Fakultät für Bauingenieur-, Geo- und Umweltwissenschaften, ISBN 978-3-935322-12-6, electronic version available at http://digbib.ubka.uni-karlsruhe.de/volltexte/1000007371, Karlsruhe, 2007).
[72] P. M. Mariano and F. Stazi, Computational aspects of the mechanics of complex materials, Arch. Comput. Meth. Engng. **12**, 392–478 (2005).
[73] P. Neff and J. Jeong, A new paradigm: the linear isotropic Cosserat model with conformally invariant curvature energy, Z. Angew. Math. Mech. **89**(2), 107–122 (2009).
[74] R. Lakes, A pathological example in micropolar elasticity, ASME J. Appl. Mech. **52**, 234–235 (1985).
[75] A. Askar and A. S. Cakmak, A structural model for a micropolar continuum, Int. J. Eng. Sci. **6**(10), 583–589 (1968).
[76] Z. P. Bazant, Micropolar medium as a model for buckling of grid frameworks, in: Developments in Mechanics, Proceedings of 12th Midwestern Mechanics Conference, (1971).
[77] Z. P. Bazant and M. Christensen, Analogy between micropolar continuum and grid frameworks under initial stress, Int. J. Solids Struct. **8**(3), 957–964 (1972).
[78] H. Ramézani, J. Jeong, I. Münch, and P. Neff, A novel linear Cosserat elasticity models with grid framework model assumptions: 3d numerical experiments of the torsion test, J. Mech. Phys. Solids (2009) Submitted.
[79] P. Neff, A. Sydow, and C. Wieners, Numerical approximation of incremental infinitesimal gradient plasticity, Int. J. Numer. Meth. Eng. **77**(3), 414–436 (2009).
[80] J. Jeong and H. Ramézani, Implementation of the finite isotropic linear Cosserat models based on the weak form, in: European Comsol Users Conference 2008, edited by Committee of European Comsol Conference in Hannover-Germany (November 2008).
[81] R. Toupin, Elastic materials with couple stresses, Arch. Rat. Mech. Anal. **11**, 385–413 (1962).
[82] R. Gauthier and W. Jahsman, A quest for micropolar constants, ASME J. Appl. Mech. **42**, 369–374 (1975).
[83] R. Gauthier and W. Jahsman, Bending of a curved bar of micropolar elastic material, ASME J. Appl. Mech. **43**, 502–503 (1976).
[84] R. Gauthier, Experimental investigations on micropolar media, in: Mechanics of Micropolar Media, edited by O. Brulin and R. Hsieh (CISM Lectures, World Scientific, Singapore, 1982), pp. 395–463.
[85] I. Alsaleh, Numerical modeling of strain localization in grannular materials using Cosserat theory enhanced with fabric properties, PhD thesis, Louisiana State University and Agricultural and Mechanical College, 2004.
[86] K. A. Alshibli, M. I. Alsaleh, and G. Z. Voyiadjis, Modelling strain localization in granular materials using micropolar theory: mathematical formulations, Int. J. Num. Anal. Meth. Geomech. **30**(15), 1501–1524 (2006).
[87] K. A. Alshibli, M. I. Alsaleh, and G. Z. Voyiadjis, Modelling strain localization in granular materials using micropolar theory: numerical implementation and verification, Int. J. Num. Anal. Meth. Geomech. **30**(15), 1525–1544 (2006).
[88] I. Münch, Ein geometrisch und materiell nichtlineares Cosserat-Modell-Theorie, Numerik und Anwendungsmöglichkeiten, PhD thesis, University of Karlsruhe (TH), October 2007, (in German).
[89] R. Lakes, On the torsional properties of single osteons, J. Biomech. **25**, 1409–1410 (1995).
[90] E. de Borst, Simulation of strain localisation: a reappraisal of the Cosserat continuum, Eng. Comput. **8**(4), 317–332 (1991).

